Host (dealumination Y zeolite)-guest (substituted heteropolyacid) nanocomposites as an efficient catalyst in the removal of methyl orange

Maryam Moosavifar (m.moosavifar90@gmail.com)
University of Maragheh https://orcid.org/0000-0003-1538-8370
Fariba Mavadat
University of Maragheh
Armen Avanes
University of Maragheh

Research Article

Keywords: Substituted heteropoly acid, Methyl orange, Photodeagaration, Template synthesis method, COD.

Posted Date: April 23rd, 2021

DOI: https://doi.org/10.21203/rs.3.rs-450554/v1

Abstract

Substituted polyoxometal encapsulated into Y zeolite was synthesized with two ratios: $H_5PMo_{10}W_1Ti_1O_{40}.XH_2O/Y$ (hereafter designated as SPY-1011, the numbers show the amount of Mo, W, Ti, respectively) and $H_5PMo_1W_{10}Ti_1O_{40}.XH_2O/Y$ (hereafter designated as SPY-1101) was synthesized using the template synthesis method. The nanocomposite materials were characterized by XRD, FT-IR, UV-Vis, FESEM, and EDS techniques. The photocatalytic activity of systems was investigated within the photodegradation of methyl orange. The W, Mo, and Ti content of the catalyst was evaluated by the ICP method. The results showed that the photocatalyst performance depends on catalyst loading, pH effect, methyl orange concentration, the type, and the number of substituted species. The chemical oxygen demand (COD) experiment indicated mineralisation of the methyl orange with 83% after 120 min irradiation. The absences of hydrazine during degradation confirmed by the amperometric experiment, in turn, showed methyl orange converted to simple inorganic materials. Photocatalytic degradation of methyl orange follows a pseudo-first-order kinetic.

Introduction

Some synthetic compounds used in various industries like textile, food, leather, paint, cosmetics, and plastic cause air contamination and wastewater and released hazardous materials [1-5]. Therefore, pollutant elimination is considered a good remedy or alternative to solve these disadvantages of these compounds. In this regard, there are a variety of conventional treatments such as chemical and biological oxidation, adsorption, electrochemical, coagulation, ion exchange, membrane separation, and advanced oxidation process [6-9]. Among them, photocatalytic degradation has attracted pronounced attention due to eco-friendly systems and compatibility with the environment [4, 10-13]. In these processes, semiconductors such as TiO_2, ZnO, WO_3, Fe_2O_3, CuO, ZrO_2, CdS, In_2O_3, and SnO_2 was used as photocatalysts that produce non-toxic products [14, 15]. However, one of the most effective photocatalysts is considered TiO_2 due to its high photocatalytic activity, biologically and chemically inert properties, and stability. Moreover, the TiO_2 possesses a large bandgap and low surface area. Also, the filtration of TiO_2 seems troublesome and costly because of its fine dispersion in the water.

In this respect, there are some strategies to overcome these disadvantages one of them, fixing TiO_2 on the support causes increases the surface area and reduces the required amount of metal oxide [16-24]. Another method in the photodegradation process is using supported and supported heteropoly acids. These systems have high Bro'nsted acidity and electron acceptor properties due to their structure, therefore facilitating photocatalytic activity [25-28]. Thus, the hybridization of heteropoly acid/TiO2/support is another manner for the photodegradation process [29]. In this respect, several researchers applied mixed metal oxide and metal sulfide to increase and improve the performance of the photocatalytic activity [23, 30-35].

In previous work, we synthesized $H_3PMo_{12}O_{40}/TiO_2/Y$ nanocomposite as a photocatalyst reagent [11]. On one hand, we entered TiO_2 in $H_3PMo_{12}O_{40}$/ Y composite for enhancing photocatalytic activity. It is worthy to note that in this case, the leaching of TiO_2 from the zeolite surface occurs. For this reason, we synthesized Ti-substituted $H_3PMo_{12-x}W_xO_{40}$ incorporated into the nanocage of zeolite for preventing Ti leaching and improving photocatalytic activity. On the other hand, we combined the advantages of photosensitivity and electron acceptor property of polyoxometal, a hollow structure of nanoporous and supporting characters of zeolite and photocatalytic activity of TiO_2 to improve contact surface, reduce bandgap and enhance photocatalytic behavior. Of course, the results were promising since first, decorated Ti on polyoxometal acts the same as TiO_2, and second, its photocatalytic reactivity becomes higher than $H_3PMo_{12}O_{40}/Y$.

Although much work is done to date, more studies need to be conducted. In previous works, metal and metal oxide was doped on TiO_2 to improve photosensitivity. But in the present study, we report Ti-doped polyoxometal for studying photocatalytic behavior. For this purpose, the receptivity property of the electron, photosensitivity, and Bronsted acidity properties of polyoxometal have been combined with the semiconductor property of Ti and the feature of zeolite support to obtain optimum conditions for photocatalytic activity performance.

Experimental

Materials and Characterizations

All materials were of the commercial reagent grade and were purchased from Sigma-Aldrich, Merck, and Fluka. NaY was synthesized using the template method. XRD patterns were achieved on an advanced Brucker-D8 diffractometer with Cu k_{a1} (l= 1.54 nm, 30 mA, 2q=5-60°). FT-IR spectra were achieved from KBr pellets using a Japan Shimadzu 8400s spectrometer. The morphology of the catalysts was achieved by FESEM on a Czech MIRA3 Tuscan microscope equipped with Energy Dispersive spectroscopy.

Preparation of zeolite–encapsulated substituted heteropoly acids

Synthesis of $H_5PMo_{10}W_1Ti_1O_{40}/Y$ (SPY-1011)

In the typical procedure, (SPY-1011) was prepared by the mixture of MoO_3 (7.2 g), WO_3 (1.16 g), and TiO_2 (0.4 g) in the suspension of zeolite (2g) followed by stirring at 308 K for 24 h. Then, H_3PO_4 was added and stirred at 95 °C for 3 h. The obtained materials were sintered and dried. Later, the solid materials were immersed in hot water, and after an hour of agitation, the samples were filtered and washed with hot water. Finally, the solid mass was treated with 0.1 M NaCl solution for the removal of unreacted metal cations.

Synthesis of $H_5PMo_1W_{10}Ti_1O_{40}/Y$ (SPY-1101)

The synthesis of SPY-1101 is similar to that of SPY-1011, except that the proportions change in this case. In this method, to a suspension of 2 g of zeolite in 150 ml of water, 11.6 g of WO_3, 0.4 g of TiO_2, and 0.72 g of MoO_3 are added and were stirred at 308 K for 24 hours. The rest of the process is similar to method 2.2.1.

General procedure for photodegradation of methyl orange by zeolite-encapsulated substituted heteropoly acids

In a typical procedure, a suspension containing catalyst and 50 mL aqueous solution of methyl orange (2.5×10^{-5} g/L) was stirred first in the dark to balance adsorption/desorption equilibrium and to remove the error of any initial adsorption effect. Then the homemade reactor was used for irradiation experiments at room temperature. The mixture was stirred magnetically during irradiation. To monitor reaction progress and degradation of methyl orange, at certain times, about 3 mL of the suspension was withdrawn and the photocatalysts were separated by filtering and using 0.45 μm disc. The photodegradation reaction progress was determined by using the band in the region of 465 nm is related to methyl orange.

Chemical oxygen demand

Chemical oxygen demand (COD) measurements were performed to determine the degradation amount of organic compounds. To this aim, COD was determined by applying standard methods including volumetric titration methodology at the beginning and the end of the experimental runs.

Results And Discussion

Preparation and characterization of zeolite–encapsulated substituted heteropoly acids

SPY-1011 and SPY-1101were synthesized into nanocage of zeolite by the ship-in-a-bottle method. Based on the formation of polyoxometal into zeolite cage, the original white color of zeolite turned and remained unchanged after purification proved that HPA encaged into zeolite cage. Besides, due to the presence of Ti in the HPA structure, its solubility is reduced. Consequently, some substituted polyoxometal remained on the external zeolite surface. Due to the high loading of complexes on the zeolite surface, peaks related to Mo-O, Mo-O-Mo, P-O, W-O_e-W, W-O_c-W, W=O_t, and Ti-O appeared and are observed in the region of 948, 795, 1080, 763, 871, 972, 760, respectively. However, the existence of a shoulder near P-O indicated the incorporation of Ti in the HPA framework (Fig. 1A). The peak in related of O-H is observed at 3430 cm^{-1}. The broadening of peaks can be assigned to the increasing in OH amount and difference in their position. Also, the presence of peaks associated with zeolite, proved the structure maintained after encaging HPA on the zeolite cage.

XRD patterns of SPY-1011 and SPY-1101 show in Fig. 1B that indicated the formation of polyoxometal in zeolite structure. Decreasing the intensity of zeolite peaks is related to the presence of Ti in heteropoly acid that causes reducing in their solubility, consequently, some of the heteropoly acids on the zeolite

surface maintain until after purification. Also, peaks in accordance with $H_3PW_{12}O_{40}$, $H_3PMo_{12}O_{40}$, WO_3, MoO_3, and TiO_2 unit proved the formation of heteropoly acid. Furthermore, a few shifts in peak position are expectable because W and Ti inserted in $H_3PMo_{12}O_{40}$ and Mo and Ti entered in $H_3PW_{12}O_{40}$ structure that affected on bond length of M-O and finally 2q.

FESEM micrograph showed cubo-octahedral unit in accordance with zeolite. So it was proved that the morphology of zeolite is retained based on the formation of polyoxometal into zeolite structure, however, the presence of some ripples on the nanoscale on the external zeolite surface can be related to substituted polyoxometal which has not been removed even after purification (Fig.1C)

FESEM-EDX spectrum of SPA-1011 and SPA-1101 confirmed the presence of zeolite and substituted heteropoly acid in the obtained photocatalyst. This, in turn, not only indicated the existence of Ti, Mo, W, P, Si, Al, Na, and O in the compound but also the ratio of elements (Fig. 1D).

Investigation of photocatalytic activity of SPY-1011

To detect the photocatalytic activity of SPY-1101 the degradation of methyl orange was tested as a function of different experimental parameters which all results are presented in Figs. 2 and 3.

The effect of catalyst amount

The effect of catalyst amount on the removal of methyl orange was studied by varying the catalyst amount from 0.03 to 0.09 g, and the results of absorbance changes in the region of 400-600 nm were brought in Fig.2A. In a low concentration of catalyst, the degradation of methyl orange does not occur completely, while in a high amount of catalyst, the adsorption of dye molecules increased. Optimum degradation was obtained with 0.05 g catalyst. However, at amounts higher than 0.05 g, photodegradation reduces because of turbidity of the solution in accordance with high amount catalyst [4, 37].

The Effect of methyl orange concentration

The photodegradation of methyl orange was studied at the different initial concentrations of methyl orange in the range of (1.5-9) ´ 10^{-5} mol/L. The results are shown in Fig. 2B. An increase in the concentration of methyl orange reduces the photodegradation process which can be related to the absorbance of light by using methyl orange rather than the catalyst, therefore, the photocatalytic efficiency reduces [38].

The effect of initial photocatalyst pH

The reaction was investigated at various solution pH. The pH of the solution is adjusted at the beginning of the reaction before irradiation. The results are shown in Fig.2C. As it is clear, the best result is obtained at pH=5. So pH plays important role in the photodegradation of methyl orange and catalytic activity affected by the strong electrostatic field. Obviously, under the alkali condition, the adsorption and

degradation of methyl orange reduce because of competition between the hydroxyl group and methyl orange ions. Therefore, it decreased the absorption of methyl orange on the catalyst surface. In acidic conditions, methyl orange converts to hydrazones due to resonance form [39].

Under the optimum conditions, decolorization of MO was investigated with SPY-1101 as a function of irradiation time. Fig.2D. shows the UV–Vis spectra of methyl orange before and after irradiation in the presence of SPY-1101. Methyl orange itself was photochemically inert in the absence of SPY-1101 which was observed without any change in the absorption spectrum. However, in the presence of photocatalyst, the absorption spectrum of methyl orange significantly reduced and after 3 hours, the degradation of MO is completed. Also, photodegradation of methyl orange was investigated in the presence of SPY-1011. The results show that SPY-1101 is better than SPY-1011 catalyst because of degradation yield (Fig. 3A).

Catalyst recovery and reusability

The reusability of the catalyst was tested in the photodegradation of methyl orange. At the end of the reaction, the catalyst was filtered, washed with water, and dried at 100°C for 3 h. The catalytic activity preserved until 4 consecutive runs and after that, was observed decreasing in photocatalytic activity (Fig. 3B).

kinetic of photodegradation

The photodegradation of MO in the presence of SPY-1101 obeys from pseudo-first-order kinetic. At low MO concentration, the rate expression is:

$$-\frac{d[c]}{dt} = k'[c]$$

k′ is the pseudo-first-order rate constant MO adsorbed on the catalyst surface and after absorption/desorption equilibrium, the concentration of MO was determined at different times. In this case, C_0 and C_t are the initial concentration at t=0 and at time t, respectively. By plotting $\ln C_t/C_0$ versus time for degradation MO, the plot is obtained linear which proved degradation of MO followed pseudo-first-order (Fig. 4).

Chemical oxygen demand (COD)

Mineralization of MO was confirmed using COD experiments. To this end, the photodegradation product was studied using COD analysis. The obtained results showed a significant COD removal (83%) after 60 min irradiation. This, in turn, indicates the mineralization of MO followed by the formation of carbon dioxide and water. Hydrazine was produced by MO photodegradation. An amperometric experiment confirmed the presence of hydrazine during photodegradation. In this case, NaOH was selected as the electrolyte. The various concentration of standard hydrazine was used to detect hydrazine signal and

ultimately, the unknown solution of hydrazine was injected and compared to that of standard hydrazine. Decreasing the flow may be related to the increasing volume of the solution without increasing in hydrazine amount (Fig. 12). It, in turn, confirms the photodegradation of methyl orange. Another proof for this claim, the measurement of COD at the beginning and the end of the experiment run were determined by the standard method by volumetric titration methodology [40].

Conclusion

In this study, the preparation of SPY-1101 and SPY-1011catalyst is performed using template synthesis. The physicochemical properties of composites characterized by XRD, FT-IR, FESEM, ICP, and EDS technique. The catalysts display efficient photoactivity in the degradation of methyl orange under UV illumination. COD experiment proved mineralization of azo dye. The kinetics of the reaction obeyed pseudo-first-order. Ti-substituted causes HPA that showed photocatalytic activity. Significantly, these catalytic systems are recoverable and can be used several times without significant loss in catalytic activity.

References

[1] M. Matouq, Z. Al-Anber, N. Susumu, T. Tagawa, H. Karapanagioti, The kinetic of dyes degradation resulted from food industry in wastewater using high frequency of ultrasound, Separation and Purification Technology, 135 (2014) 42-47.

[2] L. Ai, C. Zhang, F. Liao, Y. Wang, M. Li, L. Meng, J. Jiang, Removal of methylene blue from aqueous solution with magnetite loaded multi-wall carbon nanotube: kinetic, isotherm and mechanism analysis, Journal of Hazardous Materials, 198 (2011) 282-290.

[3] O. Tünay, I. Kabdaşlı, D. Orhon, G. Cansever, Use and minimization of water in leather tanning processes, Water science and technology, 40 (1999) 237-244.

[4] R. Aravindhan, N.N. Fathima, J.R. Rao, B.U. Nair, Wet oxidation of acid brown dye by hydrogen peroxide using heterogeneous catalyst Mn-salen-Y zeolite: a potential catalyst, Journal of Hazardous Materials, 138 (2006) 152-159.

[5] R. Kidak, N.H. Ince, Ultrasonic destruction of phenol and substituted phenols: A review of current research, Ultrasonics Sonochemistry, 13 (2006) 195-199.

[6] A. Ajmal, I. Majeed, R.N. Malik, H. Idriss, M.A. Nadeem, Principles and mechanisms of photocatalytic dye degradation on TiO_2 based photocatalysts: a comparative overview, Rsc Advances, 4 (2014) 37003-37026.

[7] N.F. Jaafar, A.A. Jalil, S. Triwahyono, M.N.M. Muhid, N. Sapawe, M.A.H. Satar, H. Asaari, Photodecolorization of methyl orange over α-Fe_2O_3-supported HY catalysts: the effects of catalyst

preparation and dealumination, Chemical engineering journal, 191 (2012) 112-122.

[8] J.-S. Wu, C.-H. Liu, K.H. Chu, S.-Y. Suen, Removal of cationic dye methyl violet 2B from water by cation exchange membranes, Journal of membrane science, 309 (2008) 239-245.

[9] C.-C. Wang, C.-K. Lee, M.-D. Lyu, L.-C. Juang, Photocatalytic degradation of CI Basic Violet 10 using TiO_2 catalysts supported by Y zeolite: an investigation of the effects of operational parameters, Dyes and Pigments, 76 (2008) 817-824.

[10] J. Sabate, M.A.A. Comparison of TiO_2 powder suspensions and TiO_2 ceramic membranes supported on glass as photocatalytic systems in the reduction of chromium(VI), Journal of Molecular Catalysis, 71 (1992) 57-68.

[11] Y. Kim, M. Yoon, TiO_2/Y-Zeolite encapsulating intramolecular charge transfer molecules: a new photocatalyst for photoreduction of methyl orange in aqueous medium, Journal of Molecular Catalysis A: Chemical, 168 (2001) 257-263.

[12] M.A. Fox, K.E. Doan, M.T. Dulay, The effect of the “Inert” support on relative photocatalytic activity in the oxidative decomposition of alcohols on irradiated titanium dioxide composites, Research on Chemical Intermediates, 20 (1994) 711-721.

[13] M. Moosavifar, S.M. Heidari, L. Fathyunes, M. Ranjbar, Y. Wang, H. Arandiyan, Photocatalytic degradation of dye pollutant over FeTPP/NaY zeolite nanocomposite, Journal of Inorganic and Organometallic Polymers and Materials, (2019) 1-8.

[14] D. Robert, Photosensitization of TiO_2 by M_xO_y and M_xS_y nanoparticles for heterogeneous photocatalysis applications, Catalysis Today, 122 (2007) 20-26.

[15] N. Talebian, M. Nilforoushan, Comparative study of the structural, optical and photocatalytic properties of semiconductor metal oxides toward degradation of methylene blue, Thin Solid Films, 518 (2010) 2210-2215.

[16] Y. Kim, M. Yoon, TiO_2/Y-Zeolite encapsulating intramolecular charge transfer molecules: a new photocatalyst for photoreduction of methyl orange in aqueous medium, Journal of Molecular Catalysis A: Chemical, 168 (2001) 257-263.

[17] Y. Xu, X. Chen, Photocatalytic reduction of dichromate over semiconductor catalysts, in, SOC CHEMICAL INDUSTRY 14 BELGRAVE SQUARE, LONDON, ENGLAND SW1X 8PS, 1990, pp. 497-498.

[18] K. Vinodgopal, S. Hotchandani, P.V. Kamat, Electrochemically assisted photocatalysis: titania particulate film electrodes for photocatalytic degradation of 4-chlorophenol, The Journal of Physical Chemistry, 97 (1993) 9040-9044.

[19] H. Chen, A. Matsumoto, N. Nishimiya, K. Tsutsumi, Preparation and characterization of TiO_2 incorporated Y-zeolite, Colloids and Surfaces A: Physicochemical and Engineering Aspects, 157 (1999) 295-305.

[20] J.-A. Cha, S.-H. An, H.-D. Jang, C.-S. Kim, D.-K. Song, T.-O. Kim, Synthesis and photocatalytic activity of N-doped TiO_2/ZrO_2 visible-light photocatalysts, Advanced Powder Technology, 23 (2012) 717-723.

[21] N. Sapawe, A. Jalil, S. Triwahyono, S. Adam, N. Jaafar, M. Satar, Isomorphous substitution of Zr in the framework of aluminosilicate HY by an electrochemical method: Evaluation by methylene blue decolorization, Applied Catalysis B: Environmental, 125 (2012) 311-323.

[22] C. McManamon, J.D. Holmes, M.A. Morris, Improved photocatalytic degradation rates of phenol achieved using novel porous ZrO_2-doped TiO_2 nanoparticulate powders, Journal of Hazardous Materials, 193 (2011) 120-127.

[23] C. Sun, L. Liu, L. Qi, H. Li, H. Zhang, C. Li, F. Gao, L. Dong, Efficient fabrication of ZrO_2-doped TiO_2 hollow nanospheres with enhanced photocatalytic activity of rhodamine B degradation, Journal of colloid and interface science, 364 (2011) 288-297.

[24] T. Kamegawa, R. Kido, D. Yamahana, H. Yamashita, Design of TiO_2-zeolite composites with enhanced photocatalytic performances under irradiation of UV and visible light, Microporous and Mesoporous Materials, 165 (2013) 142-147.

[25] S. Anandan, M. Yoon, Photocatalytic degradation of methyl orange using heteropolytungstic acid-encapsulated TiSBA-15, Solar energy materials and solar cells, 91 (2007) 143-147.

[26] M. Hu, Y. Xu, Photocatalytic degradation of textile dye X3B by heteropolyoxometalate acids, Chemosphere, 54 (2004) 431-434.

[27] M. Yoon, J.A. Chang, Y. Kim, J.R. Choi, K. Kim, S.J. Lee, Heteropoly acid-incorporated TiO_2 colloids as novel photocatalytic systems resembling the photosynthetic reaction center, The Journal of Physical Chemistry B, 105 (2001) 2539-2545.

[28] R.R. Ozer, J.L. Ferry, Investigation of the photocatalytic activity of TiO_2-polyoxometalate systems, Environmental science & technology, 35 (2001) 3242-3246.

[29] B. Bai, J. Zhao, X. Feng, Preparation and characterization of supported photocatalysts: $HPAs/TiO_2/SiO_2$ composite, Materials Letters, 57 (2003) 3914-3918.

[30] M.J. Height, S.E. Pratsinis, O. Mekasuwandumrong, P. Praserthdam, Ag-ZnO catalysts for UV-photodegradation of methylene blue, Applied Catalysis B: Environmental, 63 (2006) 305-312.

[31] X. Yang, C. Cao, L. Erickson, K. Hohn, R. Maghirang, K. Klabunde, Photo-catalytic degradation of Rhodamine B on C-, S-, N-, and Fe-doped TiO_2 under visible-light irradiation, Applied Catalysis B: Environmental, 91 (2009) 657-662.

[32] J.-H. Sun, S.-Y. Dong, J.-L. Feng, X.-J. Yin, X.-C. Zhao, Enhanced sunlight photocatalytic performance of Sn-doped ZnO for Methylene Blue degradation, Journal of Molecular Catalysis A: Chemical, 335 (2011) 145-150.

[33] L. Trandafilović, D. Jovanović, X. Zhang, S. Ptasińska, M. Dramićanin, Enhanced photocatalytic degradation of methylene blue and methyl orange by ZnO: Eu nanoparticles, Applied Catalysis B: Environmental, (2016).

[34] C. Fu, M. Li, H. Li, C. Li, X. guo Wu, B. Yang, Fabrication of Au nanoparticle/TiO_2 hybrid films for photoelectrocatalytic degradation of methyl orange, Journal of Alloys and Compounds, 692 (2017) 727-733.

[35] S. Ahluwalia, N.T. Prakash, R. Prakash, B. Pal, Improved degradation of methyl orange dye using bio-co-catalyst Se nanoparticles impregnated ZnS photocatalyst under UV irradiation, Chemical engineering journal, 306 (2016) 1041-1048.

[36] M. Moosavifar, A. Alemi, M.R. Marefat, N. Nouruzi, H. Mahmoodi, The effect of synthesis method and post-synthesis treatment on the formation of neutral Mn (II) complex into anionic zeolite structure and investigation of its catalytic activity in the epoxidation of alkenes, Journal of the Iranian Chemical Society, 11 (2014) 1561-1567.

[37] N. San, A. Hatipoğlu, G. Koçtürk, Z. Çınar, Photocatalytic degradation of 4-nitrophenol in aqueous TiO_2 suspensions: theoretical prediction of the intermediates, Journal of Photochemistry and Photobiology A: Chemistry, 146 (2002) 189-197.

[38] D. Rajamanickam, M. Shanthi, Photocatalytic degradation of an organic pollutant by zinc oxide – solar process, Arabian Journal of Chemistry, 9, Supplement 2 (2016) S1858-S1868.

[39] A.D. Bokare, R.C. Chikate, C.V. Rode, K.M. Paknikar, Iron-nickel bimetallic nanoparticles for reductive degradation of azo dye Orange G in aqueous solution, Applied Catalysis B: Environmental, 79 (2008) 270-278.

[40] A. APHA, WEF (American Public Health Association, American Water Works Association, and Water Environment Federation). 1998, Standard methods for the examination of water and wastewater, 19.

Figures

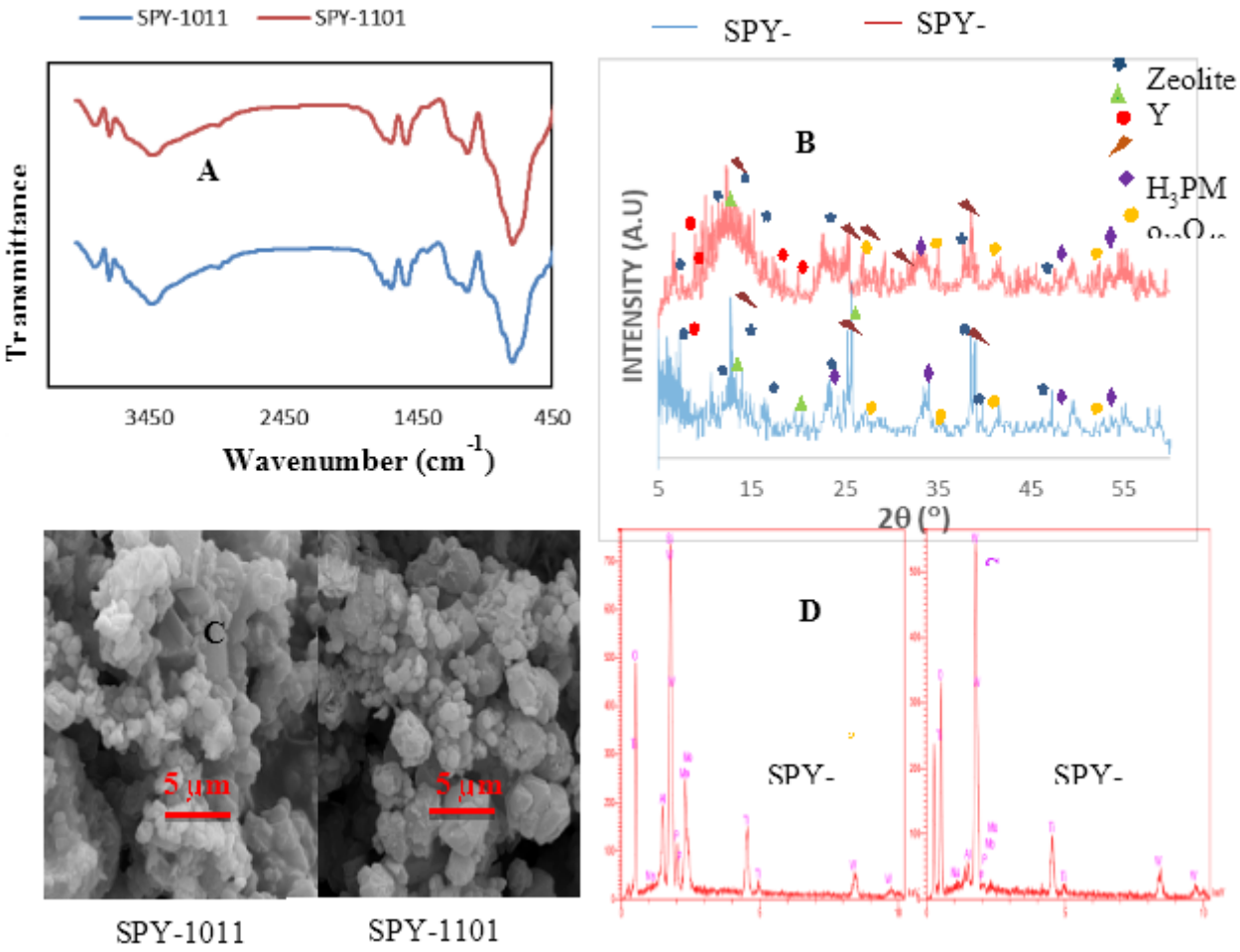

Figure 1

A) FT-IR spectra, B) XRD patterns, C) FESEM micrograph, and D) EDS analysis of SPY-1011and SPY-1101

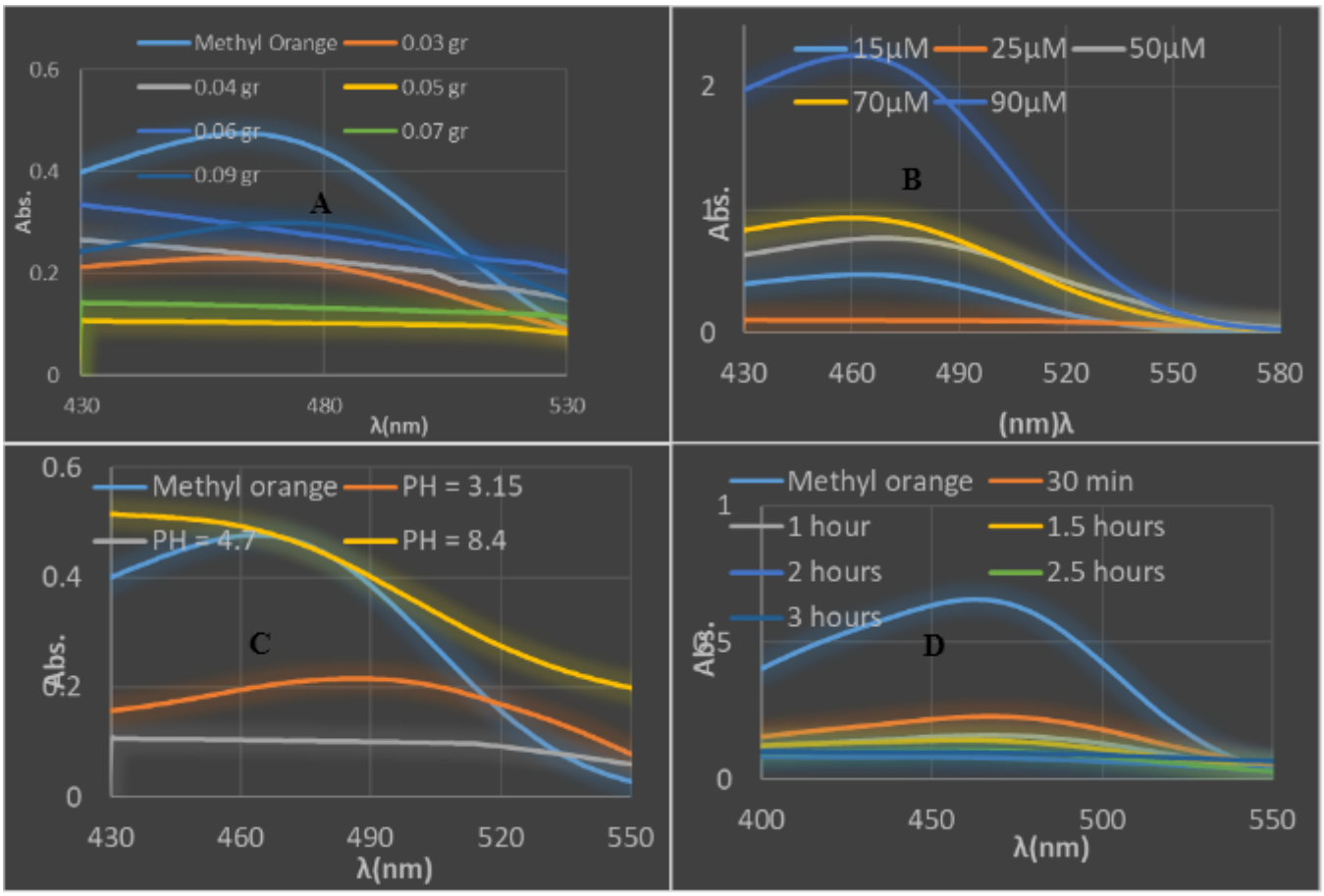

Figure 2

A. Effect of SPY-1101 catalyst amount on the photodegradation of MO. Reaction conditions: MO concentration: 25mM, reaction time: 120 min. pH=4.7, 2B) Effect of MO concentration on photodegradation process, Reaction conditions: SPY-1101 catalyst amount: 50 mg, Reaction time: 120 min, pH=4.7, 2C) Effect of pH on photodegradation process, Reaction conditions: SPY-1101 catalyst amount: 50 mg, MO concentration: 25mM, reaction time: 120 min, and 2D) Plot of the absorption change of methyl orange at 470 nm as a function of irradiation time in the presence of SPY-1101. Reaction conditions: SPY-1101 catalyst amount: 50 mg, MO concentration: 25mM, pH=4.7.

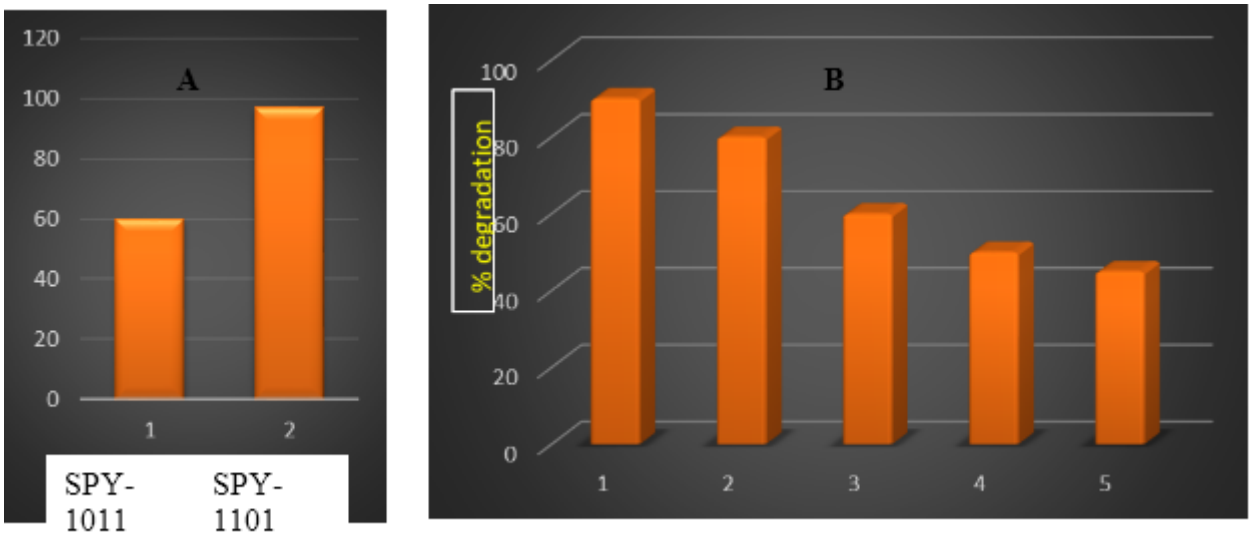

Figure 3

A) Diagram of removal MO by using of 1) SPY-1011 and 2) SPY-1101. Reaction conditions: catalyst amount: 50 mg, MO concentration: 25mM, pH=4.7. Reaction time: 120 min, 3B) Reusability of photocatalyst. Reaction conditions: SPY-1101 catalyst amount: 50 mg, MO concentration: 25mM, reaction time: 120 min, pH=4.7.

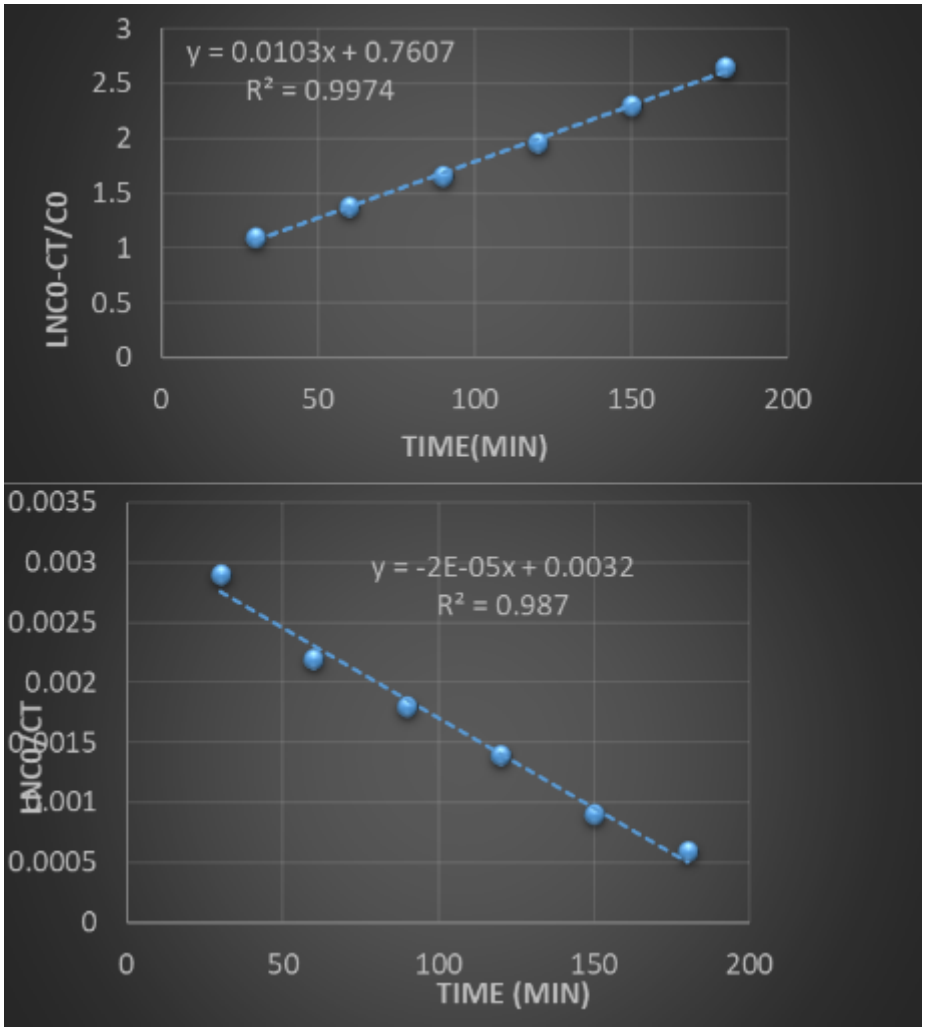

Figure 4

Plot of LnC0/Ct versus time and LnC0-Ct/C0 versus time

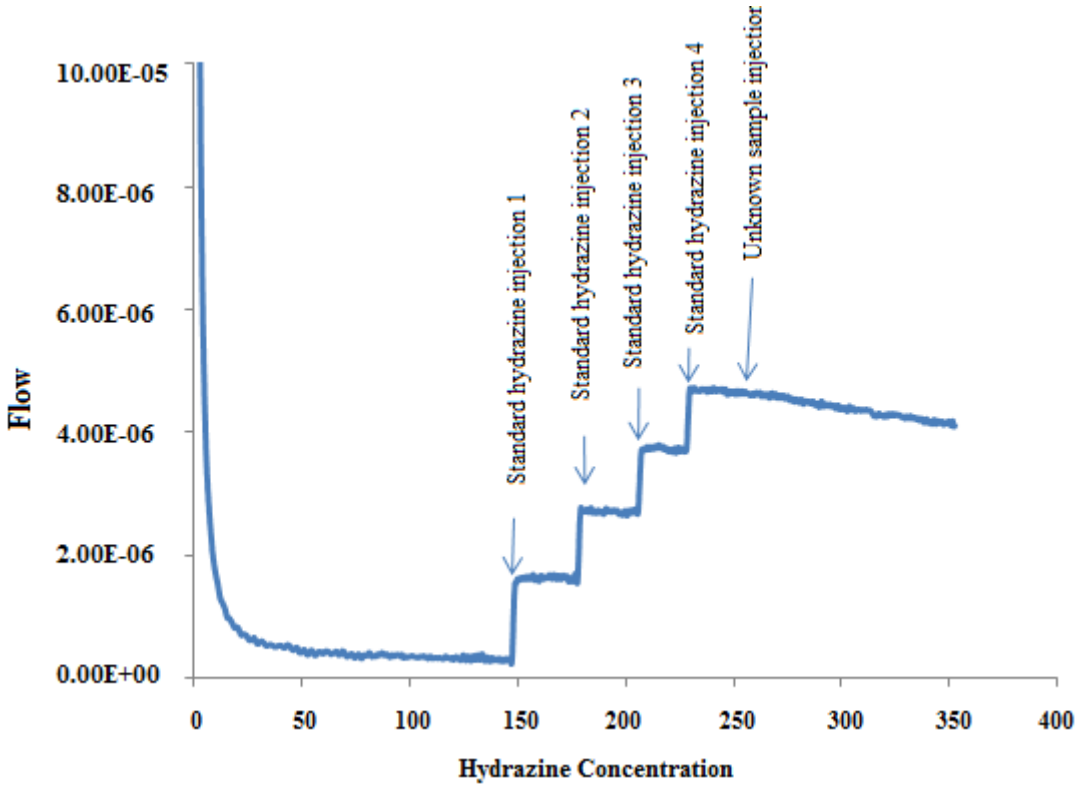

Figure 5

Plot of determination of the presence of Hydrazine in the unknown sample